Geomechanics and Engineering, *Vol. 41, No. 6 (2025) 569-582*
https://doi.org/10.12989/gae.2025.41.6.569

Coupling effect of water immersion and dynamic loading on accumulative strain and pore structure of foamed concrete

Long-Ji Zhang, Zhen-Dong Cui*, Yan-Kun Zhang and Mukhtiar Ali Soomro

State Key Laboratory of Intelligent Construction and Healthy Operation & Maintenance of Deep Underground Engineering, School of Mechanics and Civil Engineering, China University of Mining and Technology, Xuzhou, Jiangsu 221116, PR China

(*Received November 22, 2024, Revised May 23, 2025, Accepted June 10, 2025*)

Abstract. As a new type of high-speed railway subgrade filler, the deformation performance of foamed concrete under long-term traffic loading requires further research. In addition, the potential adverse effects caused by water immersion in actual environments cannot be overlooked. In this paper, a series of dynamic triaxial tests were performed to study the deformation behavior of foamed concrete samples under dry and water immersion conditions, considering the effect of dynamic stress amplitudes and confining pressures. Moreover, scanning electron microscopy was used to capture the microstructure characteristics of the foamed concrete. The pore shape coefficient and fractal dimension were introduced to explain the macroscopic deformation properties. For the dry sample subjected to dynamic loading, its resistance to deformation increases with increasing buried depth. However, the previous water immersion treatment led to the pore structure of the foamed concrete being more vulnerable to damage under subsequent dynamic loading. At this time, the accumulative deformation of the wet samples was greater than that of the dry samples, especially at the top and bottom layers. Notably, as the dynamic stress amplitude exceeded 20 kPa, a rapid growth of the accumulative deformation was observed for the samples. In addition, the pore structure characteristics of the foamed concrete under the excitation of dynamic loading experience significant variation, with the large pores splitting into small pores and the pore diameter decreasing. The pore walls of the large pores ruptured and connected with others, accompanied by an increase in the number of narrow pores. The findings in this paper contribute to a better understanding of the design and maintenance of the foamed concrete subgrade.

Keywords: accumulative strain; dynamic loading; foamed concrete; fractal dimension; pore structure; water immersion conditions

1. Introduction

Compared with ordinary concrete and traditional subgrade filler, the use of lightweight foamed concrete reduces the additional stress on the foundation (Huang *et al*. 2017, Mastali *et al*. 2018, Zhang *et al*. 2023). Moreover, foamed concrete is characterized by low cost and convenient construction (Amran *et al*. 2015, Ramamurthy *et al*. 2009). Therefore, its application in high-speed railway subgrade fillers has enormous potential. However, rainfall and groundwater seepage in the actual environment are more prone to affect foamed concrete with high porosity. Considering the rigorous requirements for smooth routes and stringent control of differential settlement for high-speed railways, the potential adverse effect of traffic loading and water immersion on the deformation performance of foamed concrete subgrades should be explored.

Currently, existing studies mainly focus on the mechanical properties of foamed concrete under monotonic loading. The effect of porosity conditions on the mechanical properties of foamed concrete under compressive loading was investigated through experiments and numerical simulations (Nguyen *et al*. 2017, Ruan *et al*. 2024). It was found that the deterioration of the mechanical characteristics coincided with increasing porosity. The uniaxial compression and tension tests were conducted on the foamed concrete with different densities, which indicated that the strength and modulus of the sample increased with increasing density (Gökçe *et al*. 2023, Zhang *et al*. 2022). In practical engineering applications, such as the tunnel support system and subgrade filler (Tan *et al*. 2017, Wang *et al*. 2012), the foamed concrete is inevitably subjected to multiaxial stress. Some scholars have investigated the influence of confining pressure on the stress-strain characteristics of the foamed concrete through triaxial compression tests. The research results indicated that the constraint action induced by confining pressure significantly affected the deformation mechanism and crack propagation of the samples (Su *et al*. 2019). Therefore, an increase in the confining pressure led to an enhancement of the peak strength and residual strength (Liu *et al*. 2022, Ma *et al*. 2019, Zhang *et al*. 2021). An empirical model was proposed to predict the compressive strength of the foamed concrete under different confining pressures (Tan *et al*. 2018). The critical state theory was employed to evaluate the failure state of the foamed concrete subjected to triaxial shear loading (Liu *et al*. 2024). A series of cyclic loading tests were performed to investigate the effect of density and

*Corresponding author, Professor
E-mail: cuizhendong@cumt.edu.cn

ISSN: 2005-307X (Print), 2092-6219 (Online)

silt content on the damage evolution of silt-based foamed concrete, indicating that the dynamic strength of the sample increases with density (Wu *et al*. 2022). Recent studies have demonstrated that admixtures significantly enhance the mechanical performance of concrete paving blocks (Abir and Sarker 2024). For instance, incorporating limestone powder improves compressive strength and stiffness by reducing porosity and enhancing microstructural stability (Mahi *et al*. 2025). Conversely, the addition of rubber crumbs to lightweight concrete has been shown to reduce compressive strength, with the magnitude of this reduction proportional to rubber content (Abhi *et al*. 2025). The peak strength of the foamed concrete decreased with increasing loading frequency. Moreover, the transformation of the failure mode under staged cyclic compression is related to the density of the sample (Rao *et al*. 2021). The dynamic triaxial tests were performed to investigate the deformation of the foamed concrete subjected to freezing-thawing cycles (Cui *et al*. 2024). Among these, few studies focused on the mechanical properties of foamed concrete under dynamic loading. Moreover, there is a research gap in the effect of water immersion on the dynamic deformation behaviors of concrete. Relevant research in this field is essential to illustrate the performance of the foamed concrete subgrade fillers.

Moreover, the microscopic tests are performed to facilitate a comprehensive understanding of the relationship between macroscopic properties and microstructure characteristics (Kim *et al*. 2020, Lee *et al*. 2022, Youn *et al*. 2023). The microstructure of the foamed concrete plays an important role in its mechanical behaviors because it influences its strength and durability (Chica *et al*. 2022, Nambiar and Ramamurthy 2007, Narayanan and Ramamurthy 2000, Zhao *et al*. 2019). It is noted that differences in the pore size distribution and porosity of foamed concrete with various densities are significant (Guo *et al*. 2021). The enhancement of sample density contributed to the occurrence of a more dense and intact pore structure, thereby improving the compressive strength (Huang *et al*. 2023). Scholars have employed the fractal dimension to quantify the complex microstructure of foamed concrete and revealed its correlation with physical properties (Stolz *et al*. 2021). The fractal theory was employed to characterize the relationship between porosity and compressive strength (Xiang *et al*. 2023). The lower strength of the sample with lower density is the reflection of more connected pores and thinner pore walls induced by the increase in foam content (Wang *et al*. 2022). The SEM images indicated that the smoother pore walls and denser skeletons contributed to the enhancement in compressive strength (Li *et al*. 2023). In contrast, the appearance of irregular combined bubbles in foamed concrete led to increased pore sizes and reduced strength (Wu *et al*. 2022, Zhang *et al*. 2021). Overall, the mechanical performance of the foamed concrete is determined by the microstructure characteristics. Systematic evaluation of the pore morphology is essential for revealing the macroscopic deformation mechanism of foamed concrete.

In practical engineering applications such as marine and road engineering, concrete structures are inevitably exposed to water during operation (Jin *et al*. 2023). The effect of water immersion on the performance of concrete has attracted attention in previous studies (He *et al*. 2022, Li *et al*. 2017, Qin *et al*. 2023, Wang *et al*. 2024). It was concluded that water immersion led to looser pore structure and weaker strength, and lots of connected pores in samples with lower densities made it more prone to be affected by water absorption (Zhang *et al*. 2024). It was observed that dry-wet cycles lead to changes in the morphological characteristics and the deterioration of the material properties (Qin *et al*. 2024). Specifically, the strength of foamed concrete decreases significantly with increasing dry-wet cycles (Shi *et al*. 2020, Wu *et al*. 2021). Due to the fact that the samples with lower density possess more connected pores and higher porosity, the loss of compressive strength becomes more significant with increasing soaking days. Compared with saturated foamed concrete, air-dried samples have a higher dynamic stress threshold (Huang *et al*. 2017). While existing research has focused predominantly on the strength of foamed concrete under monotonic loading, limited attention has been given to its dynamic deformation behavior, which is a critical property for high-speed railway subgrade fillers subjected to sustained traffic loading. Furthermore, the practical application of such subgrades necessitates considering the water infiltration condition, which leads to potential hazards to the long-term deformation performance of subgrades. An in-depth study should be carried out to sufficiently understand the accumulative deformation and microscopic characteristics of foamed concrete under a combined action of dynamic loading and water immersion conditions.

This paper aims to investigate the accumulative strain of foamed concrete under dry-wet conditions, various confining pressures, and dynamic loading amplitudes through a series of dynamic triaxial tests. Moreover, scanning electron microscopy was employed to characterize the pore structure of tested samples. Quantitative analysis of pore morphology was conducted using the pore shape coefficient and fractal dimension. The macroscopic deformation performance of foamed concrete was elucidated by systematic evaluation of the variations of the microstructure characteristics. Furthermore, the coupling effect of water immersion and dynamic loading on the pore structure evolution and the accumulative strain development was comprehensively discussed.

2. Materials and methods

2.1 Foamed concrete sample preparation

Considering the application of foamed concrete in subgrade filler, the target density of the sample prepared in this paper is selected as 600 kg/m^3 (Zhang *et al*. 2021, Zhang *et al*. 2020). The water-cement ratio (W/C) of the foamed concrete was taken as 0.6 in the test. According to the technical specification for foamed mixture lightweight soil filling engineering (JGJ-T341-2014), the mix proportions of the samples were calculated, as summarized in Table 1. Herein, the ordinary P.O. 42.5 Portland cement

Table 1 Mix proportion and mechanical parameters of foam concrete

Target density (kg/m^3)	Water cement ratio	Cement content (kg/m^3)	Water content (kg/m^3)	Foaming agent (L/m^3)	Flow value (mm)	Dry density (kg/m^3)	Compressive strength at 7d (MPa)	Compressive strength at 28d (MPa)
600	0.6	350	210	0.56	182	570	0.62	0.73

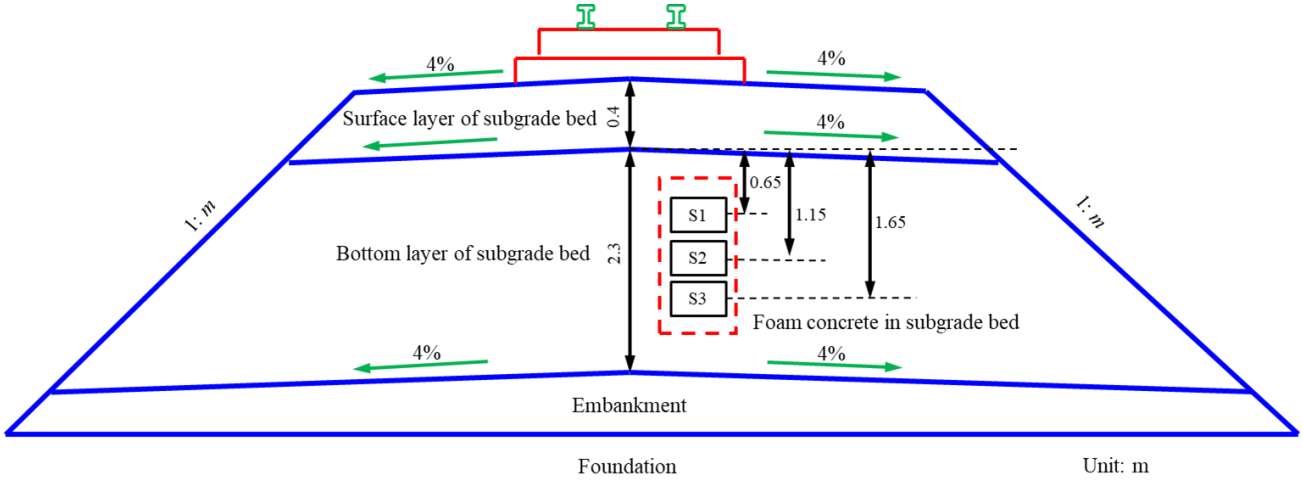

Fig. 1 Different position of foamed concrete in ballastless track subgrade

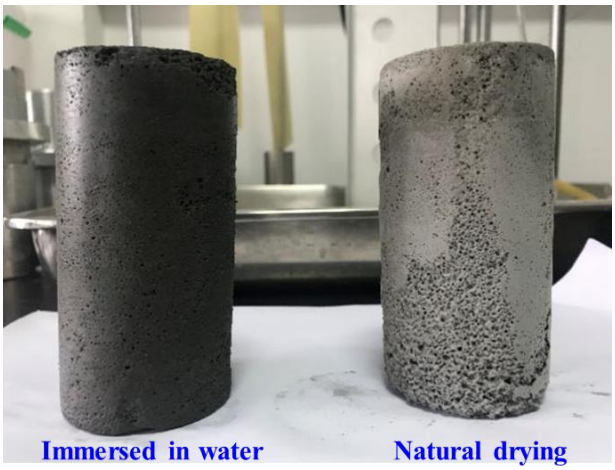

(a) Foam concrete sample

(b) Apply dynamic loading

Fig. 2 Sample preparation and test procedure

was used as the raw material. The physical foaming method was employed to prepare the sample by mixing water, cement and prefabricated foam without adding minerals and additives. The prefabricated foaming agent, with a foaming ratio of 22, was diluted with water at a ratio of 1:60 by volume. At this time, the foam half-life was measured as 22 h. Subsequently, the air was introduced through mechanical agitation to produce lots of bubbles. Ultimately, the prepared foam was added to the cement slurry, and the sample was poured into a cylinder with a diameter of 50 mm and a height of 100 mm, satisfying the requirement of dynamic triaxial tests. The cast sample was cured at room temperature for 1d to achieve hardening, and then it was placed in a standard curing box for 28 d. The compressive strength of the foamed concrete is summarized in Table 1.

2.2 Dynamic triaxial test

The GDS dynamic triaxial apparatus, with a maximum loading frequency of 5 Hz and a maximum axial force of 5 kN, is adopted in the experiments. It has a high-precision data acquisition and a convenient test control system, capable of dynamic monitoring of the whole test process. According to the design specification for a high-speed railway (TB10621-2014), the self-weight of the CRTSIII plate ballastless track is 13.7 kN/m^3. The thickness of the surface layer of the subgrade bed is 0.4 m, and the weight of the fine-graded gravel used here is 19.5 kN/m^3. The thickness of the bottom layer of the subgrade bed is 2.3 m, where the density of the foamed concrete filler ρ is 580 kg/m^3. The different positions of the foamed concrete

sample in the ballastless track subgrade are illustrated in Fig. 1. Foamed concrete samples under various in-situ stress states corresponding to different buried depths of 0.65 m, 1.15 m and 1.65 m were selected as the research objects.

The vertical and confining stresses were calculated by $\sigma_v = 13.7 + 19.5 \times 0.4 + \gamma_c h$ and $\sigma_c = K_0 \sigma_v$, where the unit weight of the foamed concrete $\gamma_c = \rho g = 5.68\ kN/m^3$, and the coefficient of lateral pressure K_0=0.4 (Tiwari *et al*. 2017). Therefore, the vertical effective stresses σ_v' corresponding to the S1, S2 and S3 positions were 25.2 kPa, 28.1 kPa and 30.9 kPa, respectively. The corresponding confining pressures σ_c' were 10.1 kPa, 11.2 kPa and 12.4 kPa, respectively. In the dynamic triaxial test, the calculated in-situ stress was first applied to the specimen, followed by the application of dynamic loading. Considering the measured dynamic stress at the ballastless track subgrade and the amplification effect induced by the smoothness of the high-speed rail track (Bian *et al*. 2014), the dynamic loading amplitudes applied in the dynamic triaxial tests are taken as 10 kPa, 20 kPa and 30 kPa. The natural drying and wetting samples were prepared to investigate the effect of water immersion conditions on the dynamic behavior of foamed concrete. The wetting sample was immersed in water for 24 hours before the excitation of dynamic loading by the dynamic triaxial apparatus. The test procedure is illustrated in Fig. 2. To simulate the traffic loading of a high-speed train, the sinusoidal load was employed with a frequency of 3.5 Hz (Huang *et al*. 2017, Zhang *et al*. 2023), and the number of loading cycles N was 5000.

2.3 Scanning electron microscopy experiment

To further investigate the effect of water immersion conditions, confining pressure and dynamic loading on the pore structure of the foamed concrete, SEM tests were carried out to capture pictures of the microscopic pore structure of the foamed concrete samples. Following the dynamic triaxial tests under varying loading and water immersion conditions, ten cubic samples with a side length of 1 cm were extracted from distinct parts of the foam concrete sample. To comprehensively characterize the global and local characteristics of the pore structures, five images were taken for each sample under varying magnifications (20, 40, 60, 100, and 200). These images were further processed by Image Pro Plus software to count the area and perimeter of the pores.

3. Experimental results and discussions

3.1 Analysis of accumulative strain

3.1.1 Effect of confining pressure

The accumulative strain of naturally dried foamed concrete under different confining pressures is illustrated in Fig. 3(a). The accumulative strain of the sample under a confining pressure of 10.1 kPa after N=5000 is 1.06%, while the total deformation of the sample under confining pressures of 11.2 kPa and 12.4 kPa is 0.691% and 0.619%,

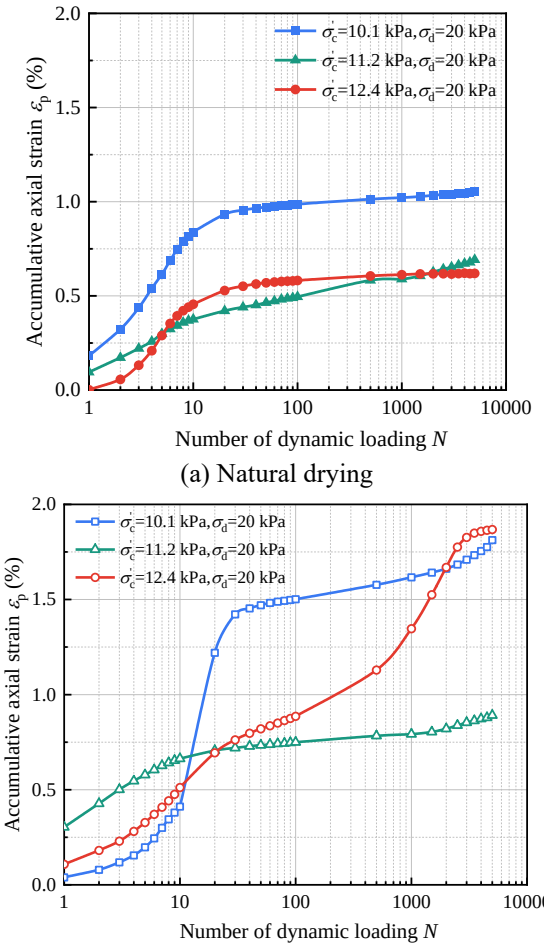

Fig. 3 Variations of accumulative strain with number of cycles under various confining pressures

respectively. It is evident that the accumulative strain decreases with increasing confining pressure. At N=10, the strains under confining pressures of 10.1 kPa, 11.2 kPa and 12.4 kPa reach 79.5%, 54.3% and 73.5% of the ultimate deformation, respectively. At N=100, the strains of these samples are 93.5%, 71.6% and 93.9% of the total deformation, respectively. Due to the existence of a large number of pores inside the foamed concrete, the pores are compacted under the continuous action of dynamic loading, accompanied by the rapid development of accumulative strain. However, the strength and stiffness of the sample are large, and the applied dynamic loading is relatively small.

The strain of the sample increases at the initial stage but gradually tends to stabilize. Moreover, the development of accumulative strain is inhibited by increasing confining pressure (Liu *et al*. 2024, Su *et al*. 2019). A decreasing confining pressure results in an increase in the growth rate of accumulative strain and total deformation. Due to the lower confining pressure in the shallow subgrade bed, the foamed concrete subgrade filler at the top layer will produce greater deformation under the dynamic loading.

3.1.2 Effect of dynamic loading

The accumulative strain of naturally dried foamed

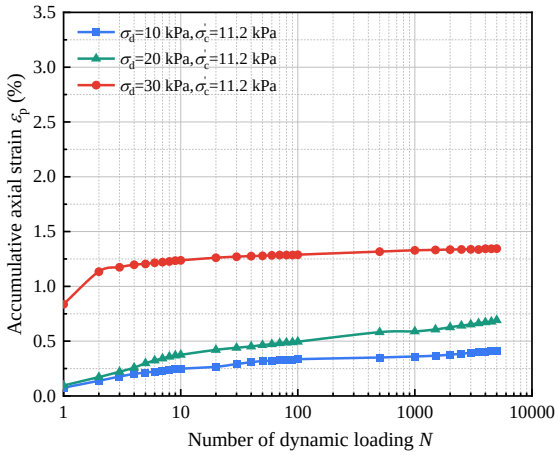

(a) Natural drying

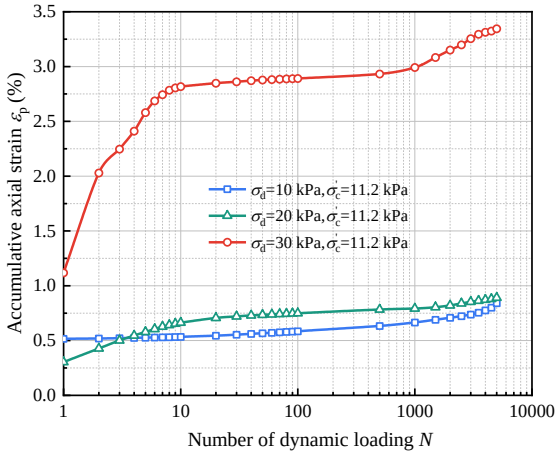

(b) Immersed in water for 24 h

Fig. 4 Variations of accumulative strain with number of cycles under various dynamic loading amplitudes

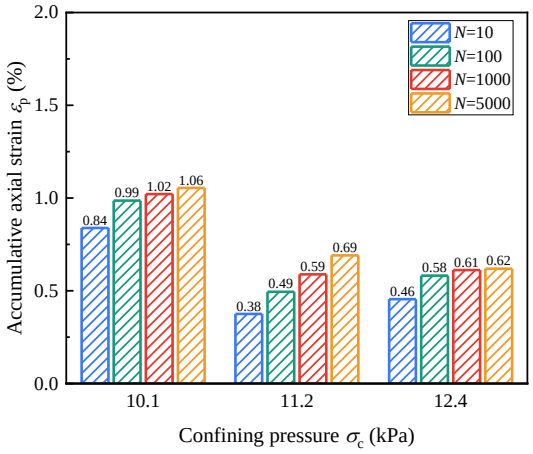

(a) Natural drying

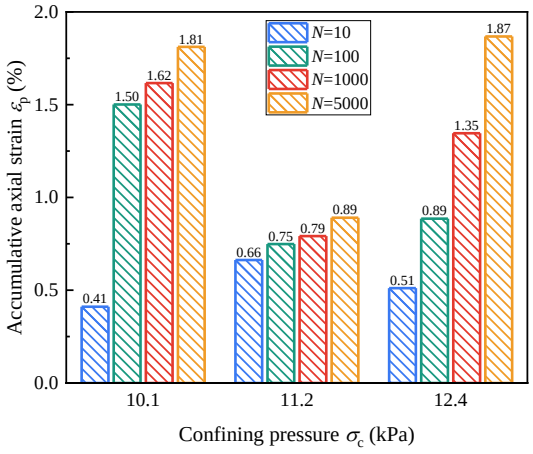

(b) Immersed in water for 24 h

Fig. 5 Variations of accumulative strain with confining pressures under different loading times

concrete under different dynamic loading amplitudes is illustrated in Fig. 4(a). During the first 500 cycles of loading, the accumulative strain experiences significant development. Under the dynamic loading of 10 kPa, 20 kPa and 30 kPa, the accumulative strain of the sample is 0.35%, 0.58% and 1.32%, respectively. After that, for the samples with dynamic loading amplitudes of 10 kPa and 20 kPa, the development of the strain still maintains a rapid growth rate.

For the sample subjected to 30 kPa, the strain undergoes stable increase after N=500. Ultimately, the accumulative strain of the sample is 0.41%, 0.49% and 1.34%. It is observed from Fig. 4(a) that the development of the accumulative strain of the sample under 30 kPa before N=10 is more abrupt compared with that subjected to lower dynamic loading amplitudes. The damage to the foam concrete sample caused by dynamic loading is apparent at the initial stage, resulting in obvious deformation of the sample. As the loading cycles increase, the incremental damage caused by dynamic loading becomes limited. Consequently, the accumulative strain of the sample gradually tends to stabilize in the end. It can be concluded that increasing dynamic loading leads to a surge in deformation and its growth rate (Cui *et al*. 2024, Wu *et al*. 2022).

3.1.3 Effect of water immersion conditions

Fig. 3(b) illustrates the variations of the accumulative strain of wet foamed concrete sample under different confining pressures. Fig. 5 shows the relationship between the confining pressure and strain under different loading times. For the wet sample under a confining pressure of 10.1 kPa, the growth rate of deformation is slow at the initial stage, and the accumulative strain is lower than that of the dry sample. At N=100, the strain of the wet sample reaches 1.5% and maintains a rapid growth rate. However, the strain of the dry sample is only 0.987% and remains stable. After N=5000, the accumulative strain of the wet sample reaches 1.81%, which is 1.71 times greater than that of the dry sample. In summary, water immersion deteriorates the resistance of foamed concrete to dynamic loading, resulting in a dramatic increase in deformation and its accumulative rate.

For the sample with a confining pressure of 11.2 kPa, the promoting effect of water immersion on the accumulative strain is more significant at the initial stage than that in the case of 10.1 kPa. At N=10, the accumulative strain of the wet sample reaches 0.663%, while it reaches 0.375% for the dry sample. The results demonstrate that the development tendencies of the deformation of the two

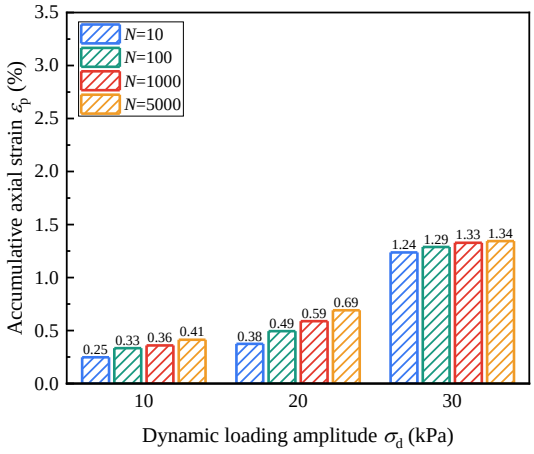

(a) Natural drying

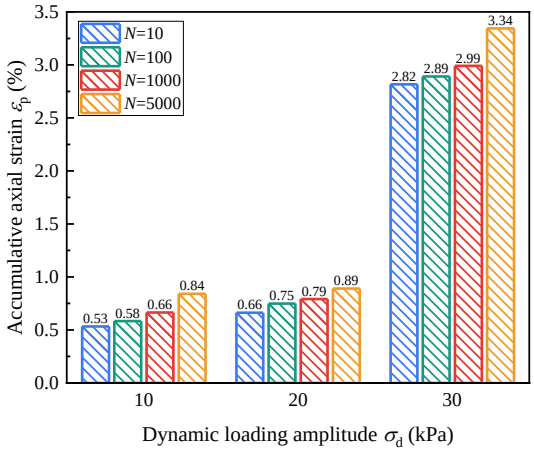

(b) Immersed in water for 24 h

Fig. 6 Variations of accumulative strain with dynamic loading amplitudes under different loading times

samples are essentially similar. However, there exists an inhibiting effect of the confining pressure on the deformation behavior of foamed concrete subjected to dynamic loading. It is evident that increasing the confining pressure results in a decrease in the accumulative strain, which is accompanied by an attenuated growth rate. After N=5000, the strain of the wet sample reached 0.891%, 1.29 times that of the dry sample. Compared with the sample under a confining pressure of 10.1 kPa, the difference between the dry and wet samples under 11.2 kPa significantly decreases.

For the wet sample with a confining pressure of 12.4 kPa, the growth rate of deformation is greater than that of the dry sample at the beginning of dynamic loading. At N=100, the accumulative strain of the wet sample reaches 0.886%, while it reaches 0.582% for the dry sample. With the continuous action of cyclic loading, the discrepancy between the two samples becomes more remarkable. Ultimately, the accumulative strain of the wet sample is 1.87%, 3.02 times that of the dry sample, which is the most significant among those of the samples subjected to different confining pressures. The degradation of the dynamic properties induced by water immersion and the restriction of the confining pressure have a coupling effect on the deformation behavior of the foamed concrete. With increasing confining pressure, the internal pore structure of the foamed concrete sample becomes more vulnerable due to the prior immersion process. As a result, more significant deformation is observed under the excitation of dynamic loading.

Fig. 4(b) illustrates the variations of the accumulative strain of the wet foamed concrete sample subjected to different dynamic loading amplitudes. Fig. 6 indicates the connection between the dynamic loading and strain under different loading times. For the wet sample under 10 kPa at N=10, the accumulative strain reaches 2.14 times that for the dry sample. At N=5000, the strain of the wet foamed concrete sample is 0.841%, which is 2.03 times that of the dry sample. There is a significant difference in the development tendency of the accumulative strain between the wet and dry samples when the dynamic loading amplitude is limited. With a dynamic loading amplitude of 30 kPa, the accumulative strain of the wet sample rapidly builds up during the first ten loading cycles and reaches 2.82%, while it is 1.24% for the dry sample. Subsequently, the growth rate of the deformation gradually decreases, especially for the dry foamed concrete, for which the strain reaches 1.34% in the end, while it is 3.34% for the wet sample. To summarize, prior immersion in water leads to deterioration of the mechanical properties of the foamed concrete. Moreover, the pore structure of the sample becomes fragile after immersion, resulting in more significant deformation with increasing dynamic loading amplitude. The accumulative strain of the dry sample under a dynamic loading of 30 kPa increases by 93.9% compared with that under 20 kPa, and increases by 223.7% compared with that under 10 kPa. However, for the wet sample, the proportions are 274.9% and 297.1%, respectively. Therefore, the combined action of prior water immersion and dynamic loading can cause more severe damage than individual actions.

3.2 Analysis of pore structure

Fig. 7 illustrates that the pore structure of the undisturbed foamed concrete samples is generally smooth and intact. Regions D and F represent punctate and flocculent cracks in the pores. Region E represents the areas without pore structure. Figs. 8 and 9 show SEM images of the foamed concrete samples under different conditions at magnifications of 20 and 100, respectively. There is a significant difference in the pore size within the sample. Large pores are relatively independent, and small pores are concentrated. The internal pores of the sample are divided into independent pores, aggregated pores and connected pores according to morphological characteristics. Independent pores are characterized by a nearly circular shape, with no significant holes in their inner surface. Aggregated pores are usually large and irregular, formed by two or more bubbles (Gökçe *et al*. 2023). It is divided into the spindle type, composite type, and gourd type. Spindle-shaped pores are formed by bubbles of similar size, as shown in A in Fig. 8. Composite pores are formed by multiple bubbles, which are usually irregularly shaped and

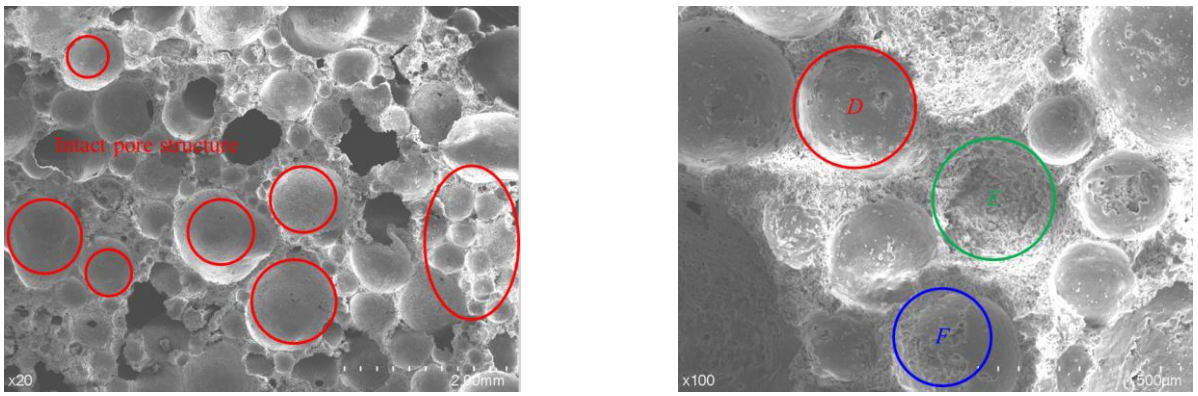

(a) Magnification of 20 times (b) Magnification of 100 times

Fig. 7 SEM image of undisturbed foamed concrete sample

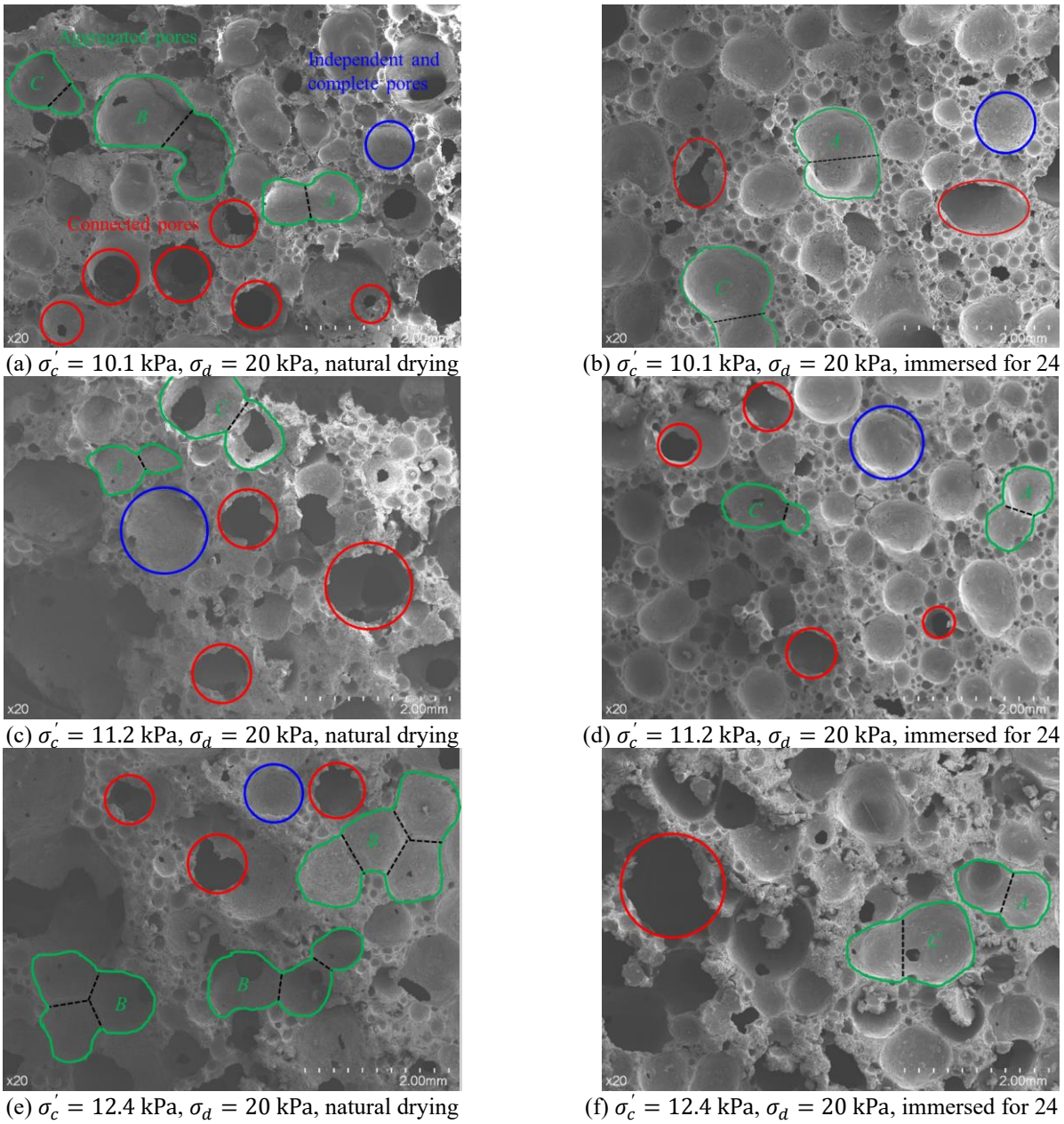

(a) $\sigma_c^{'} = 10.1$ kPa, $\sigma_d = 20$ kPa, natural drying (b) $\sigma_c^{'} = 10.1$ kPa, $\sigma_d = 20$ kPa, immersed for 24 h

(c) $\sigma_c^{'} = 11.2$ kPa, $\sigma_d = 20$ kPa, natural drying (d) $\sigma_c^{'} = 11.2$ kPa, $\sigma_d = 20$ kPa, immersed for 24 h

(e) $\sigma_c^{'} = 12.4$ kPa, $\sigma_d = 20$ kPa, natural drying (f) $\sigma_c^{'} = 12.4$ kPa, $\sigma_d = 20$ kPa, immersed for 24 h

Fig. 8 SEM image of foamed concrete sample with magnification of 20 times

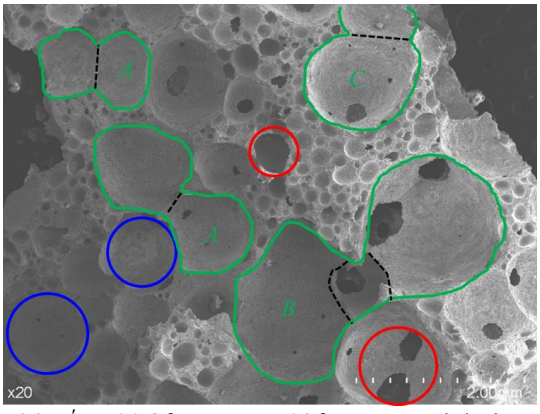

(g) $\sigma_c^{'} = 11.2$ kPa, $\sigma_d = 10$ kPa, natural drying

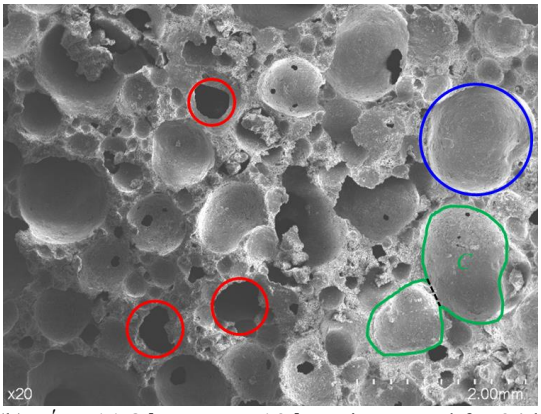

(h) $\sigma_c^{'} = 11.2$ kPa,$\sigma_d = 10$ kPa, immersed for 24 h

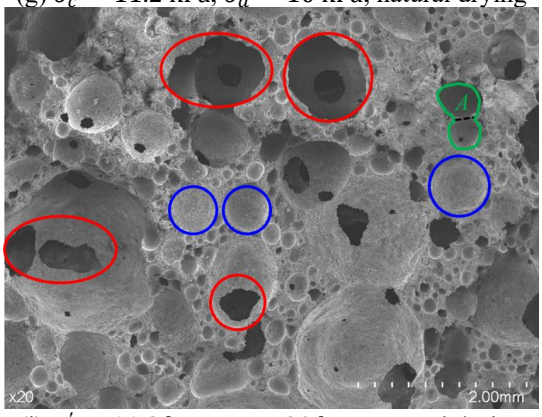

(i) $\sigma_c^{'} = 11.2$ kPa, $\sigma_d = 30$ kPa, natural drying

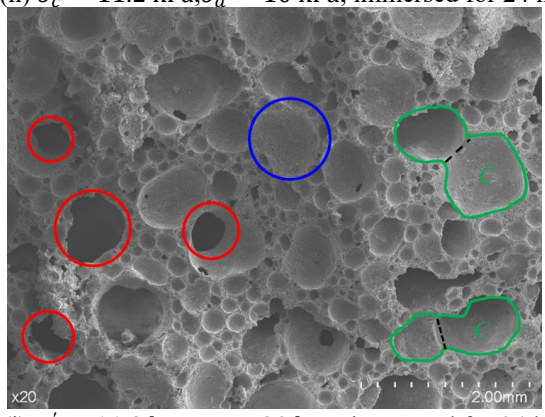

(j) $\sigma_c^{'} = 11.2$ kPa,$\sigma_d = 30$ kPa, immersed for 24 h

Fig. 8 Continued-

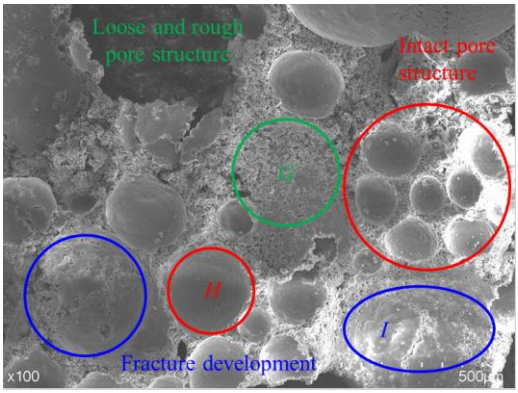

(a) $\sigma_c^{'} = 10.1$ kPa, $\sigma_d = 20$ kPa, natural drying

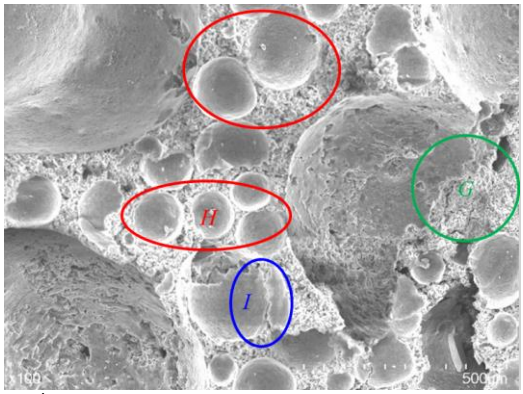

(b) $\sigma_c^{'} = 10.1$ kPa, $\sigma_d = 20$ kPa, immersed for 24 h

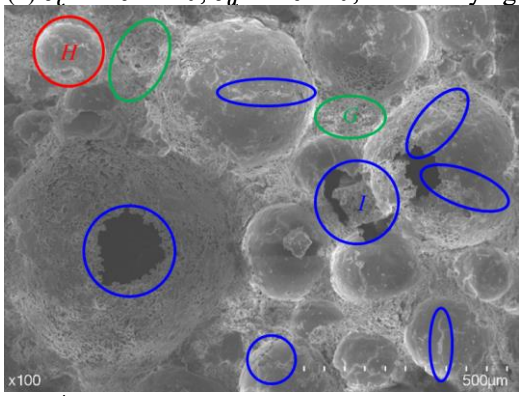

(c) $\sigma_c^{'} = 11.2$ kPa, $\sigma_d = 20$ kPa, natural drying

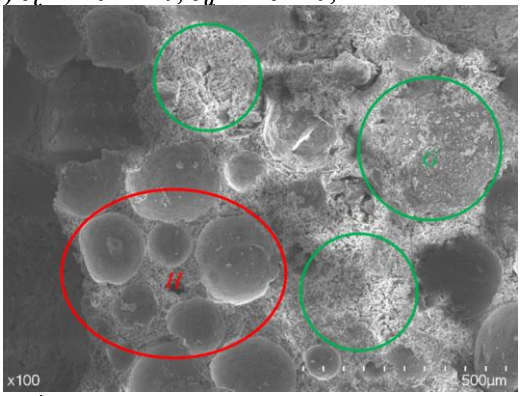

(d) $\sigma_c^{'} = 11.2$ kPa, $\sigma_d = 20$ kPa, immersed for 24 h

Fig. 9 SEM image of foamed concrete sample with magnification of 100 times

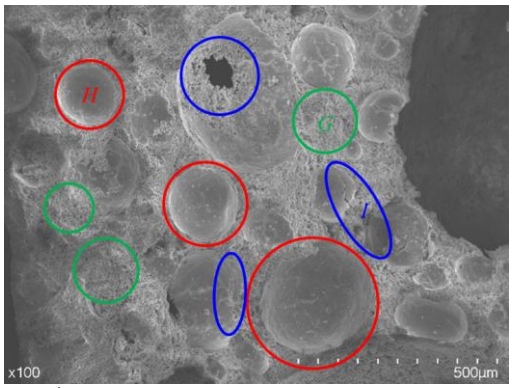

(e) $\sigma_c^{'}$ = 12.4 kPa, σ_d = 20 kPa, natural drying

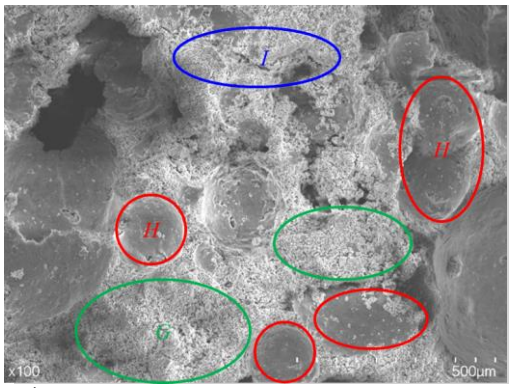

(f) $\sigma_c^{'}$ = 12.4 kPa, σ_d = 20 kPa, immersed for 24 h

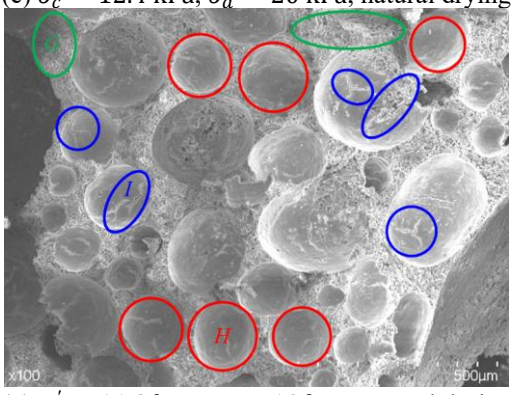

(g) $\sigma_c^{'}$ = 11.2 kPa, σ_d = 10 kPa, natural drying

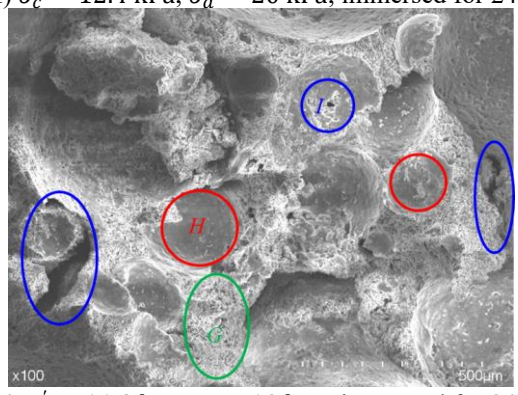

(h) $\sigma_c^{'}$ = 11.2 kPa,σ_d = 10 kPa, immersed for 24 h

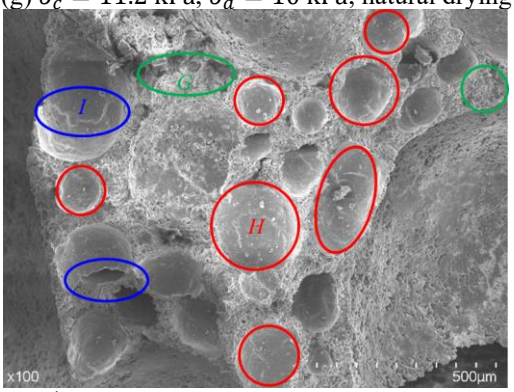

(i) $\sigma_c^{'}$ = 11.2 kPa, σ_d = 30 kPa, natural drying

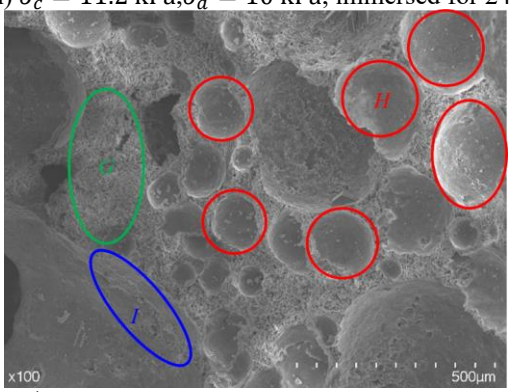

(j) $\sigma_c^{'}$ = 11.2 kPa,σ_d = 30 kPa, immersed for 24 h

Fig. 9 Continued-

have a larger area than other types of pores, as shown in B in Fig. 8. Gourd-shaped pores are formed by large and small bubbles, as shown in C. In addition, protrusions are observed on the inner wall of the aggregated pores, as shown by the black dashed line in Fig. 8. This is due to the incomplete polymerization of bubbles before the hardening of the slurry. The prominent feature of connected pores is that there are holes in the inner wall. Furthermore, the damage to the pore structure induced by the dynamic loading is always accompanied by the rupture of bubbles and the generation of connected pores. In Fig. 9, regions H, G and I represent the intact pores, the area without pores, and the cracks and holes in the pore structure, respectively. After experiencing the dynamic loading, the completeness and uniformity of the pore structure decrease significantly, accompanied by the occurrence of numerous linear cracks.

It can be concluded that the dynamic loading results in the development of cracks and the generation of connected pores.

It is observed from the SEM images at different scales that the change in the pore structure of the samples before and after undergoing cyclic loading reflects the overall shape of the pores, the development degree of cracks, and the degree of particle breakage. Increasing the dynamic loading amplitude leads to damage to the pore structure, ultimately causing a significant increase in the accumulative strain. For the wet sample, the water infiltrated its internal pore structure. On the one hand, the pore structure becomes loose due to the reduction in the cohesion among the particles. On the other hand, the excitation of cyclic loading results in the generation of excess pore water pressure. Therefore, the deformation ability of the concrete skeleton

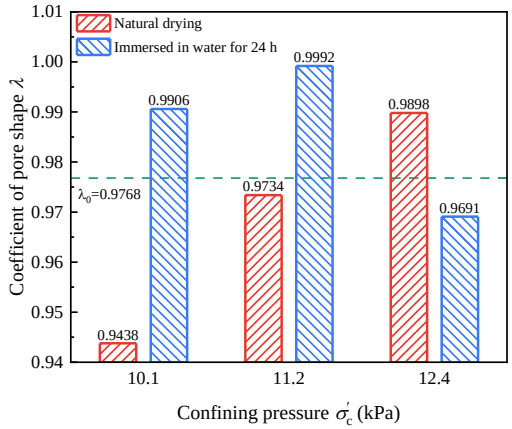

(a) Different confining pressures

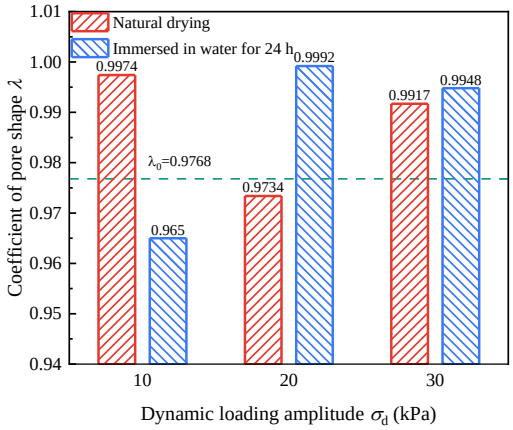

(b) Different dynamic loading amplitudes

Fig. 10 Coefficient of pore shape of foamed concrete sample

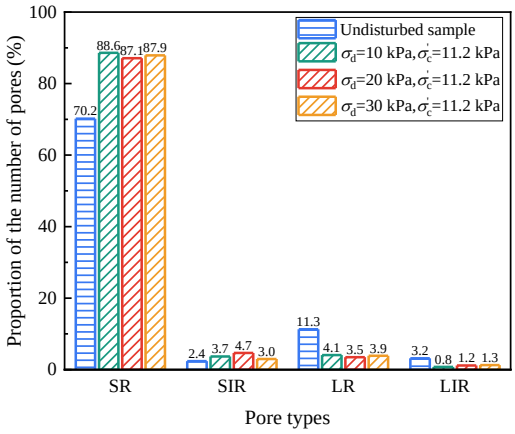

(a) Natural drying

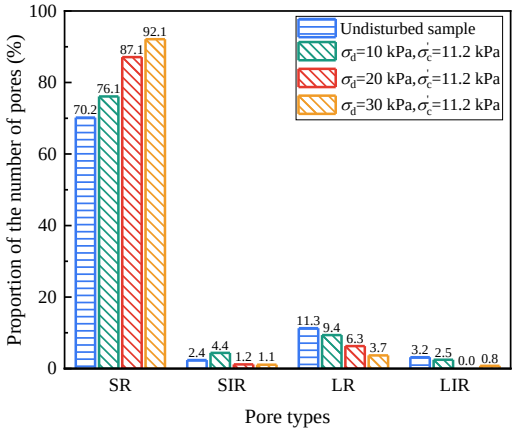

(b) Immersed in water for 24 h

Fig. 11 Proportion of different types of pores under different dynamic loading amplitudes

is restricted, which is not conducive to the resistance of the sample to dynamic loading. Compared with that of the dry sample, the damage to the pore structure of the wet sample induced by dynamic loading is severe, and the development of deformation is apparent. In summary, the combined effect of water immersion and dynamic loading deteriorates the ability of foamed concrete to resist deformation. The change in the internal pore structure is related to the mechanical properties.

3.3 Analysis of pore shape coefficient

The SEM images of the foamed concrete sample were processed using gray binarization, which made the pore structure more intuitive than those in the original images. Thus, essential parameters such as the area, diameter and perimeter of the pores were conveniently measured to realize the quantitative analysis of the microscopic characteristics. Herein, the coefficient of the pore shape shown in formula (1) is introduced to determine the relationship between the pore shape and pore size (Zhang and Cui 2017).

$$\lambda = \frac{2\pi\sqrt{A/\pi}}{P} \tag{1}$$

where A is the area of the pores; and P is the perimeter of the pores.

Figs. 10(a) and 10(b) show the average pore shape coefficients of the foamed concrete samples subjected to the different confining pressures and dynamic loading amplitudes. For the majority of the pores in the undisturbed sample, the diameters d are in the range of 40 μm ~400 μm, and the shape coefficients λ are distributed between 0.9 and 1.1 with an average value $\lambda_0 = 0.9768$. Small pores ($d < 400\ \mu m$) occupy 72.6% of the total number of pores but only 22.1% of the total area. There are only a few large pores ($d > 600\ \mu m$), accounting for 14.5% of the total number but occupying 69.4% of the total area. Although small pores are superior in number, the mechanical properties of foamed concrete samples are dominated by large pores.

After experiencing cyclic loading, the shape coefficients of the pores range from 0.95 to 1.05, and the diameter ranges from 55 μm to 400 μm. Compared with the undisturbed sample, there are more pores with λ less than 0.9 in a similar range of pore diameters, especially for large pores. To be specific, cyclic loading results in an increase in the number of small pores and narrow pores in the samples. The reason is that the pore size of medium-sized pores decreases due to the compression of dynamic loading, while

the pore walls of some adjacent large pores are damaged and connected into narrow or more irregularly shaped pores. In this paper, the pores are divided into four categories based on the pore diameter and shape coefficient: regular small pores (SR) with $0.9 < \lambda < 1.1$ and $d < 400\ \mu m$, irregular small pores (SIR) with $\lambda < 0.9$ and $d < 400\ \mu m$, regular large pores (LR) with $0.9 < \lambda < 1.1$ and $d > 600\ \mu m$, and irregular large pores (LIR) with $\lambda < 0.9$ and $d > 600\ \mu m$. The distributions of various types of pores under different dynamic loading amplitudes and confining pressures are shown in Figs. 11 and 12, respectively.

It is found that the proportion of small pores increases while the proportion of regular large pores decreases, and the change in irregular large pores is negligible. The generation of axial strain during dynamic triaxial compression tests results in the compression of internal pores and a reduction in pore size. The results indicate that under the same experimental conditions, the proportion of irregular small pores in the wet samples decreases, accompanied by an increase in the percentage of large pores and regular small pores. As illustrated in Sect. 3.1.3, the accumulative deformation of the sample subjected to prior water immersion is greater than that of the dry sample. This phenomenon is mainly due to the densification of small pores and the breakage of large pores. Water immersion has a significant weakening effect on the structure of large pores. Some large pores are more prone to be compressed or separated into multiple pores under dynamic loading (Liu *et al*. 2024), which reasonably explains the higher proportion of regular small pores in wet samples. In summary, the internal structure of foamed concrete becomes fragile after water immersion. As a result, it is more prone to be broken under dynamic loading.

Based on the distribution of pore types under different confining pressures, it is found that the sample with the lowest confining pressure has the highest proportion of irregular small and large pores, while the sample with the highest confining pressure has the highest proportion of regular large pores. In general, a decrease in the proportion of large pores is accompanied by the development of deformation. For the dry sample with a confining pressure of 11.2 kPa, although the proportion of large pores is lower than that with a confining pressure of 10.1 kPa, the accumulative strain is smaller than that with a lower confining pressure. The development of the accumulative strain of the foamed concrete sample under dynamic loading is mainly manifested as the compression and damage of large pores in perspective of the microscopic level.

There is no significant difference in the proportion of the four types of pores in the dry samples under dynamic loading amplitudes in the range of 10 kPa~30 kPa. However, the effect of the loading amplitude on the change in the pore types of the wet samples is significant. The research results mentioned in Sect. 3.1.2 indicate that the accumulative strain of the sample increases significantly with increasing dynamic loading amplitude. However, the internal pores of the dry sample are relatively complete, and the deformation mainly focuses on the end of the sample in

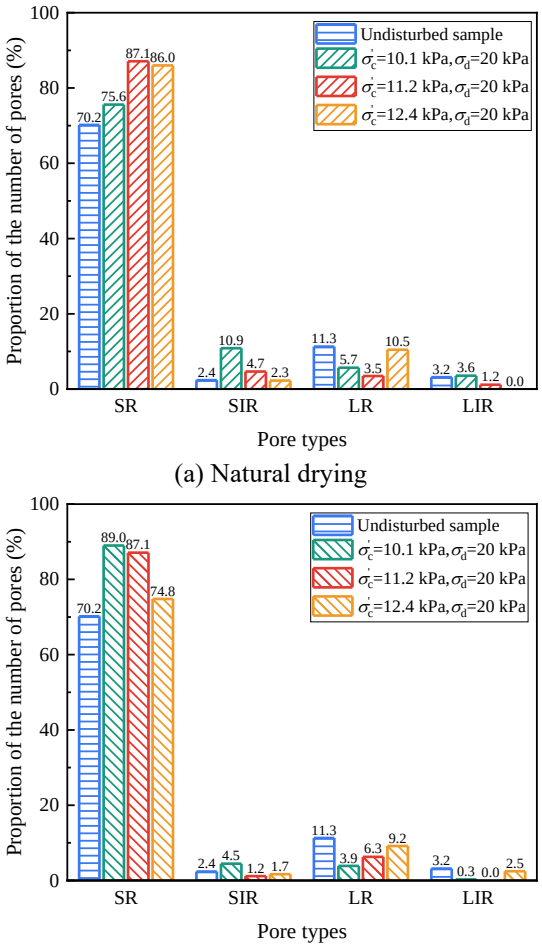

Fig. 12 Proportion of different types of pores under different confining pressures

contact with the dynamic triaxial apparatus. It is difficult to adequately characterize the behavior of the axial strain of a dry sample by the changes in its pore types. The stability of the pores decreases and the overall pore structure becomes fragile due to the action of water immersion (Zhang *et al*. 2024). This phenomenon is beneficial for the generation of homogeneous deformation during cyclic loading. In conclusion, the consistency of deformation and the vulnerability of the pore structure in wet samples commonly result in apparent changes in the pore types. This reasonably explains the effect of water immersion on the mechanical properties of foamed concrete, including the reduction in the resistance to dynamic loading and the enhancement of the ability to produce homogeneous deformation.

3.4 Analysis of fractal dimension

There exists a lot of developed internal pores with irregular shapes in the foamed concrete samples. Herein, the fractal dimension is introduced to quantitatively describe the complexity of the pore structure, as calculated by formula (2) (Meisel 1991). Similarly, the area and perimeter of the pores are important parameters for obtaining the fractal dimension.

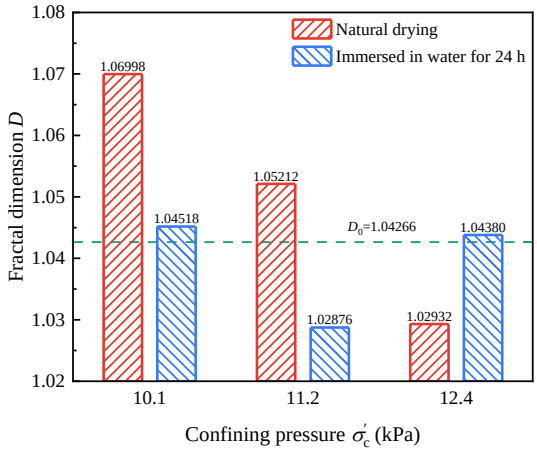

(a) Different confining pressures

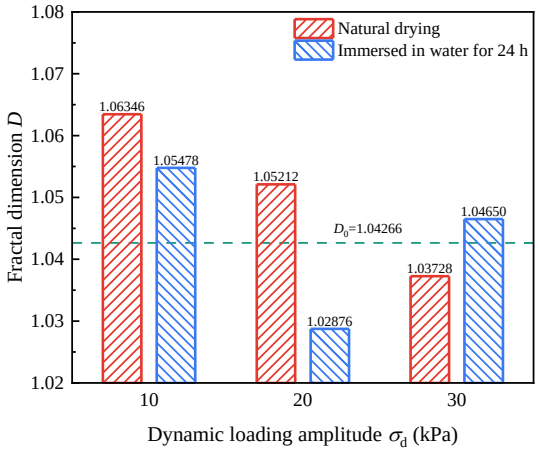

(b) Different dynamic loading amplitudes

Fig. 13 Fractal dimension of foamed concrete sample

$$\lg P = \frac{D}{2}\lg A + C \tag{2}$$

where D is the fractal dimension; and C is the fitting parameter.

Figs. 13(a) and 13(b) show the fractal dimensions of the foamed concrete samples under the different confining pressures and dynamic loading amplitudes, respectively. It is observed that the fractal dimension of the dry sample decreases with increasing dynamic loading (Cui *et al*. 2024). A similar phenomenon is found for the samples subjected to various confining pressures. The compression of the samples induced by dynamic loading and confining pressure leads to the densification of the pores. Consequently, the size of the pores becomes closer with more regular features. For the wet samples, the fractal dimension decreases first and then increases with increasing dynamic loading and confining pressure. The larger the fractal dimension, the more significant the complexity and inhomogeneity of the pore structures in foamed concrete samples (Huang *et al*. 2023). The weakening effect of water immersion results in the pore structure being more prone to compression. Therefore, the fractal dimension for the wet sample is lower than that for the dry sample. However, when the confining pressure reaches 12.4 kPa or the dynamic loading reaches 30 kPa, the fractal dimension of the wet sample exhibits a slump. This indicates that the appearance of cracks, broken particles, and connected pores leads to an increase in the irregularity of the pores. The burgeoning deformation reflects the damage to the microstructure, which agrees well with the results illustrated in Figs. 5 and 6.

In conclusion, the generation of the accumulative strain is mainly due to the densification of the pores and the displacement of the particles under dynamic loading amplitudes of 10 kPa and 20 kPa. The change in fractal dimension is determined by the enhancement of the similarity among the pores. The disturbance of the pore structure under the dynamic loading of 30 kPa is significant, affecting the stability and strength of the foamed concrete, especially for the wet sample. A widening gap in the size and shape of the pore structure gradually builds up. Therefore, the irregularity of the pores plays a dominant role in the behavior of the microstructure.

4. Conclusions

In this study, the effects of water immersion conditions, confining pressures, and dynamic loading amplitudes on the accumulative strain of foamed concrete were investigated using a dynamic triaxial apparatus. Subsequently, microscopy images of the samples were obtained by SEM at different magnifications. The shape coefficient and fractal dimension of the pores were employed to analyze the characteristics of the microstructure. The research results reveal the relationship between the deformation behavior and the microscopic structure. The main conclusions are as follows.

- As the dynamic stress amplitude exceeds 20 kPa, the development of the accumulative strain of foamed concrete becomes more rapid. For the dry sample, its resistance to dynamic deformation increases with increasing buried depth. However, compared with the dry sample, the accumulative deformation of the wet samples is greater, especially at the top and bottom subgrade layers.
- The change in pore type is due to the densification and damage of the pore structure induced by dynamic loading. The appearance of cracks, broken particles, and connected pores in the sample is accompanied by the evolution of the accumulative strain. The microscopic characteristics of foamed concrete are related to its dynamic deformation behaviors.
- The previous water immersion results in the microstructure of the foamed concrete being more susceptible to the damage induced by subsequent dynamic loading. The pore structure characteristics experience pronounced change, with the large pores splitting into small pores and the pore diameter decreasing. The pore walls of the large pores rupture and connect with others, accompanied by an increase in the number of narrow pores.
- The combined effect of water immersion and dynamic loading results in more severe deterioration of the

macroscopic deformation properties of the foamed concrete. For the foamed concrete subgrade fillers, it is necessary to reasonably set up the drainage facilities, focusing on the deformation performance of the surface and bottom subgrade.

Acknowledgments

This study was supported by the National Natural Science Foundation of China (Grant No. 52378381), the National Key Research and Development Program (Grant No. 2017YFC1500702), the Postgraduate Research & Practice Innovation Program of Jiangsu Province (Grant No. KYCX24_2805), the Graduate Innovation Program of China University of Mining and Technology (Grant No. 2024WLJCRCZL053) and China University of Mining and Technology Open Sharing Fund for Large-scale Instruments and Equipment (Grant No. DYGX-2024-41).

References

Abhi, A.N., Nafiuzzaman, M., Uzzaman, M.R., Rabby, A.A. and Rafid, M.M.R. (2025), "Compressive strength Bbehavior of recycled concrete with fine aggregate replacement using rubber crumb", *Smart Green Mater.*, **1**(2), 22-34. https://doi.org/10.70028/sgm.v1i2.36.

Abir, A.H. and Sarker, M.A.H. (2024), "Effect of different admixtures on mechanical properties of concrete paving bBlock: a comparative study", *Smart Green Mater.*, **2**(1), 99-113. https://doi.org/10.70028/sgm.v1i2.13.

Amran, Y.H.M., Farzadnia, N., Abang Ali, A.A. (2015), "Properties and applications o and foamed concrete; a review", *Constr. Build. Mater.*, **101**, 990-1005. https://doi.org/10.1016/j.conbuildmat.2015.10.112.

Bian, X.C., Jiang, H.G., Cheng, C., Chen, Y.M., Chen, R.P. and Jiang, J.Q. (2014), "Full-scale model testing on a ballastless high-speed railway under simulated train moving loads", *Soil Dyn. Earthq. Eng.*, **66**, 368-384. https://doi.org/10.1016/j.soildyn.2014.08.003.

Chica, L., Mera, C., Sepúlveda-Cano, L.M. and Alzate, A. (2022), "Porosity estimation and pore structure characterization of foamed cement paste using non-specialized image digital processing", *Mater. Struct.*, **55**(7), 189. https://doi.org/10.1617/s11527-022-02031-6.

Cui, Z.D., Zhang, L.J., Fan, K.K. and Yuan, L. (2024), "Coupling effect of freezing-thawing cycles and dynamic loading on the accumulative deformation and microstructure of foam concrete", *Mater. Struct.*, **57**(6), 136. https://doi.org/10.1617/s11527-024-02409-8.

Gökçe, H.S., Öksüzer, N., Kamiloğlu, H.A., Eyüboğlu, M. and Yılmaz, F. (2023), "The Toughness of Polypropylene Fiber-Reinforced Foam Concrete under Various Uni- and Tri-Axial Compression Loads", *KSCE J. Civ. Eng.*, **27**(7), 2982-2992. https://doi.org/10.1007/s12205-023-1345-9.

Guo, Y.Z., Chen, X.D., Chen, B., Wen, R.K. and Wu, P. (2021), "Analysis of foamed concrete pore structure of railway roadbed based on X-ray computed tomography", *Constr. Build. Mater.*, **273**, 121773. https://doi.org/10.1016/j.conbuildmat.2020.121773.

He, R., Li, S.Y., Fu, C.Q., Zhou, K.W. and Dong, Z. (2022), "Influence of cyclic drying-wetting and carbonation on oxygen diffusivity of cementitious materials: Interpretation from the perspective of microstructure", *J. Mater. Civ. Eng.*, **34**(10), 04022256. https://doi.org/10.1061/(ASCE)MT.1943-5533.0004414.

Huang, J.J., Su, Q., Zhao, W.H., Li, T. and Zhang, X.X. (2017), "Experimental study on use of lightweight foam concrete as subgrade bed filler of ballastless track", *Constr. Build. Mater.*, **149**, 911-920. https://doi.org/10.1016/j.conbuildmat.2017.04.122.

Huang, W., Chen, X.D., Feng, L., Ji, T., Ning, Y.J. and Wang, J. (2023), "Experimental investigation of mechanical behavior and microstructural properties in roadbed foam concrete at different densities and correlation analysis", *Case Stud. Constr. Mater.*, **19**, e02565. https://doi.org/10.1016/j.cscm.2023.e02565.

Jin, Y.L., Wang, X.Q., Huang, W., Li, X. and Ma, Q. (2023), "Mechanical and durability properties of hybrid natural fibre reinforced roadbed foamed concrete", *Constr. Build. Mater.*, **409**, 134008. https://doi.org/10.1016/j.conbuildmat.2023.134008.

JGJ-T341 (2014), Technical Code for Application of Foam Concrete, China Architecture & Building Press; Beijing, China.

Kim, J.S., Chung, S.Y., Han, T.S., Stephan, D. and Elrahman, M.A. (2020), "Correlation between microstructural characteristics from micro-CT of foamed concrete and mechanical behaviors evaluated by experiments and simulations", *Cement Concrete Compos.*, **112**, 103657. https://doi.org/10.1016/j.cemconcomp.2020.103657.

Lee, D.M., Lee, S.C. and Yoo, S.W. (2022), "Workability and compressive behavior of PVA-ECC with CNTs", *Geomech. Eng.*, **29**(3), 311-320. https://doi.org/10.12989/gae.2022.29.3.311.

Li, M.G., Tan, H.B., He, X.Y., Jian, S.W., Li, G.Y., Zhang, J.J., Deng, X.F. and Lin, X.L. (2023), "Enhancement in compressive strength of foamed concrete by ultra-fine slag", *Cement Concrete Compos.*, **138**, 104954. https://doi.org/10.1016/j.cemconcomp.2023.104954.

Li, Y., Liu, X.F. and Li, J.Q. (2017), "Bond properties of FRP-concrete interface with nano-modified epoxy resin under wet-dry cycles", *KSCE J. Civ. Eng.*, **21**(4), 1379-1385. https://doi.org/10.1007/s12205-016-0921-7.

Liu, M.P., Liu, Z.K., Wang, K., Ma, C.Y., Zhang, H.B. and Zhuang, P.Z. (2022), "Strength and deformation performances of silt-based foamed concrete under triaxial shear loading", *J. Build. Eng.*, **60**, 105237. https://doi.org/10.1016/j.jobe.2022.105237.

Liu, M.P., Zhang, H.B., Lv, B., Du, C. and Wang, J.Z. (2024), "Investigation on the yield and failure criterion of foamed concrete", *J. Build. Eng.*, **84**, 108604. https://doi.org/10.1016/j.jobe.2024.108604.

Mahi, M.S.H., Ridoy, T.A., Nibir, M.F.A. and Sheikh, M.S. (2025), "Limestone Powder in Concrete Mixes: A Review of Mechanical Enhancements", *Smart Green Mater.*, **1**(2), 11-21. https://doi.org/10.70028/sgm.v1i2.25.

Ma, S.S., Chen, W.Z. and Zhao, W.S. (2019), "Mechanical properties and associated seismic isolation effects of foamed concrete layer in rock tunnel", *J. Rock Mech. Geotech. Eng.*, **11**(1), 159-171. https://doi.org/10.1016/j.jrmge.2018.06.006.

Mastali, M., Kinnunen, P., Isomoisio, H., Karhu, M. and Illikainen, M. (2018), "Mechanical and acoustic properties of fiber-reinforced alkali-activated slag foam concretes containing lightweight structural aggregates", *Constr. Build. Mater.*, **187**, 371-381. https://doi.org/10.1016/j.conbuildmat.2018.07.228.

Meisel, L.V. (1991), "Perimeter-area analysis, the slit-island method and the fractal characterization of metallic fracture surfaces", *J. Phys. D: Appl. Phys.*, **24**(6), 942. https://doi.org/10.1088/0022-3727/24/6/020.

Nambiar, E.K.K. and Ramamurthy, K. (2007), "Air-void characterisation of foam concrete", *Cement Concrete Res.*, **37**(2), 221-230.

https://doi.org/10.1016/j.cemconres.2006.10.009.
Narayanan, N. and Ramamurthy, K. (2000), "Structure and properties of aerated concrete: a review", *Cement Concrete Compos.*, **22**(5), 321-329. https://doi.org/10.1016/S0958-9465(00)00016-0.
Nguyen, T.T., Bui, H.H., Ngo, T.D. and Nguyen, G.D. (2017), "Experimental and numerical investigation of influence of air-voids on the compressive behaviour of foamed concrete", *Mater. Des.*, **130**, 103-119. https://doi.org/10.1016/j.matdes.2017.05.054.
Qin, S.F., Wang, L.H., Liu, J., Xu, X.L., Li, Z. and Wang, X.P. (2024), "3D Morphology Characteristics of Concrete Interfaces under Seawater Dry-Wet Cycles", *J. Mater. Civ. Eng.*, **36**(2), 04023580. https://doi.org/10.1061/JMCEE7.MTENG-16564.
Qin, Y., Men, B., Liang, D., Geng, K., Zhang, X., Zhou, H. and Liu, R. (2023), "Energy evolution of concrete with cold joint under the action of sulfate dry-wet cycles with loading", *J. Build. Eng.*, **68**, 106098. https://doi.org/10.1016/j.jobe.2023.106098.
Ramamurthy, K., Kunhanandan Nambiar, E.K. and Indu Siva Ranjani, G. (2009), "A classification of studies on properties of foam concrete", *Cement Concrete Compos.*, **31**(6), 388-396. https://doi.org/10.1016/j.cemconcomp.2009.04.006.
Rao, F.R., Zhang, Z., Ye, G.B. and Liu, J.T. (2021), "Mechanical behavior and assessment of foamed cement paste under staged cyclic loading", *Mater. Struct.*, **54**(5), 182. https://doi.org/10.1617/s11527-021-01781-z.
Ruan, B., Li, J.C., Gan, Y.D. and Huang, J.L. (2024), "Mesoscopic simulation of the mechanical behaviour of foam concrete subjected to large compressive deformation", *Constr. Build. Mater.*, **418**, 135367. https://doi.org/10.1016/j.conbuildmat.2024.135367.
Shi, X.N., Huang, J.J. and Su, Q. (2020), "Experimental and numerical analyses of lightweight foamed concrete as filler for widening embankment", *Constr. Build. Mater.*, **250**, 118897. https://doi.org/10.1016/j.conbuildmat.2020.118897.
Stolz, J., Boluk, Y. and Bindiganavile, V. (2021), "Correlating the cellular network, in foamed concrete containing ash, with their physical properties", *Can. J. Civ. Eng.*, **48**(12), 1620-1629. https://doi.org/10.1139/cjce-2019-0265.
Su, B.Y., Zhou, Z.W., Li, Z.Q., Wang, Z.H. and Shu, X.F. (2019), "Experimental investigation on the mechanical behavior of foamed concrete under uniaxial and triaxial loading", *Constr. Build. Mater.*, **209**, 41-51. https://doi.org/10.1016/j.conbuildmat.2019.03.097.
Tan, X.J., Chen, W.Z., Liu, H.Y. and Chan, A.H.C. (2018), "Stress-strain characteristics of foamed concrete subjected to large deformation under uniaxial and triaxial compressive loading", *J. Mater. Civ. Eng.*, **30**(6), 04018095. https://doi.org/10.1061/(ASCE)MT.1943-5533.0002311.
Tan, X.J., Chen, W.Z., Liu, H.Y., Chan, A.H.C., Tian, H.M., Meng, X.J., Wang, F.Q. and Deng, X.L. (2017), "A combined supporting system based on foamed concrete and U-shaped steel for underground coal mine roadways undergoing large deformations", *Tunn. Undergr. Sp. Tech.*, **68**, 196-210. https://doi.org/10.1016/j.tust.2017.05.023.
TB10621 (2014), Code for Design of High Speed Railway, China Railway Press Beijing; Beijing, China.
Tiwari, B., Ajmera, B., Maw, R., Cole, R., Villegas, D. and Palmerson, P. (2017), "Mechanical properties of lightweight cellular concrete for geotechnical applications", *J. Mater. Civ. Eng.*, **29**(7), 06017007. https://doi.org/10.1061/(ASCE)MT.1943-5533.0001885.
Wang, H., Chen, W.Z., Tan, X.J., Tian, H.M. and Cao, J.J. (2012), "Development of a new type of foam concrete and its application on stability analysis of large-span soft rock tunnel", *J. Cent. South Univ.*, **19**(11), 3305-3310. https://doi.org/10.1007/s11771-012-1408-4.
Wang, S., Lim, J.L.G. and Tan, K.H. (2022), "Strength, shrinkage and creep of lightweight cementitious composite incorporating carbon nanofibers", *Mater. Struct.*, **55**(7), 196. https://doi.org/10.1617/s11527-022-02025-4.
Wang, Z.C., Liu, S.Y., Wu, K., Li, M.Y., Zhang, X. and Huang, L. (2024), "Durability against dry–wet and freeze–thaw cycles of alkali residue-based foamed concrete", *Mater. Struct.*, **57**(3). https://doi.org/10.1617/s11527-024-02318-w.
Wu, J.Q., Lv, C., Pi, R.D., Zhang, H.B., Bi, Y.F., Song, X.G. and Wang, Z. (2021), "The stability and durability of silt-based foamed concrete: A new type of road engineering material", *Constr. Build. Mater.*, **304**, 124674. https://doi.org/10.1016/j.conbuildmat.2021.124674.
Wu, J.Q., Wang, J., Liu, M.P., Zhuang, P.Z., Zhang, H.B. and Song, X.G. (2022), "Dynamic properties of silt-based foamed concrete as filler in subgrade", *J. Mater. Civ. Eng.*, **34**(10), 04022241. https://doi.org/10.1061/(ASCE)MT.1943-5533.0004398.
Xiang, G.S., Song, D.Q., Li, H.J., Jalal, F.E., Wang, H. and Zhou, Y.K. (2023), "Investigation on preparation and compressive strength model of steel slag foam concrete", *J. Build. Eng.*, **72**, 106548. https://doi.org/10.1016/j.jobe.2023.106548.
Youn, S., Ball, A., Fulks, C., Lee, S. and Na, S. (2023), "Effects of activated carbon on the compressive strength of Portland cement concrete", *Geomech. Eng.*, **33**(1), 19-27. https://doi.org/10.12989/gae.2023.33.1.019.
Zhang, H.B., Liu, M.P., Shuo, Z., Zhao, Z.Z., Sun, Y.H., Song, X.G., Wang, H., Zhang, X.Y. and Wu, J.Q. (2021), "An experimental investigation of the triaxial shear behaviors of silt-based foamed concrete", *Case Stud. Constr. Mater.*, **15**, e00713. https://doi.org/10.1016/j.cscm.2021.e00713.
Zhang, H.B., Qi, X.L., Wan, L.Y., Zuo, Z.W., Ge, Z., Wu, J.Q. and Song, X.G. (2020), "Properties of silt-based foamed concrete: A type of material for use in backfill behind an abutment", *Constr. Build. Mater.*, **261**, 119966. https://doi.org/10.1016/j.conbuildmat.2020.119966.
Zhang, H.B., Wang, J., Liu, Z.K., Ma, C.Y., Song, Z.S., Cui, F., Wu, J.Q. and Song, X.G. (2024), "Strength characteristics of foamed concrete under coupling effect of constant compressive loading and freeze-thaw cycles", *Constr. Build. Mater.*, **411**, 134565. https://doi.org/10.1016/j.conbuildmat.2023.134565.
Zhang, H.B., Wang, J., Wang, C., Liu, M.P. and Wu, J.Q. (2023), "Using foamed concrete layer to optimize the design of pavement and subgrade structures: From the perspectives economy and durability", *Arab. J. Sci. Eng.*, **48**(10), 12859-12874. https://doi.org/10.1007/s13369-023-07606-1.
Zhang, K.P., Zhang, X.H. and Zhou, S.H. (2023), "Analysis on dynamic behavior of 400 km/h high-speed train system under differential settlement of subgrade", *Eng. Struct.*, **278**, 115521. https://doi.org/ 10.1016/j.engstruct.2022.115521.
Zhang, S., Liu, M.P., Wang, C., Zhang, H.B. and Wu, J.Q. (2022), "Compression, Unloading-reloading, and tension mechanical behaviors of Silt-based foamed concrete under uniaxial loading", *Constr. Build. Mater.*, **347**, 128558. https://doi.org/10.1016/j.conbuildmat.2022.128558.
Zhang, Z.L. and Cui, Z.D. (2017), "Analysis of microscopic pore structures of the silty clay before and after freezing-thawing under the subway vibration loading", *Environ. Earth Sci.*, **76**(15), 528. https://doi.org/10.1007/s12665-017-6879-z.
Zhao, X.Q., Zhao, G., Li, J.W. and Zhang, P. (2019), "Unconfined compressive strength property and its mechanism of construction waste stabilized lightweight soil", *Geomech. Eng.*, **19**(4), 307-314. https://doi.org/10.12989/gae.2019.19.4.307.

GC